ARTICLE | OPEN ACCESS

Discovery

To Cite:
Fasiku TB, Awodunmila AJ. The influence of corrugation amplitude on entropy production of turbulent flow in outward corrugated converging pipes. *Discovery* 2026; 62: e8d3237
doi:

Author Affiliation:
[1]Department of Physics, Ajayi Crowther University, Oyo-Town, Nigeria
[2]Centre for Energy and Research Development, Obafemi Awolowo University, Ile-Ife, Nigeria

***Corresponding author:**
Taiwo Bukola Fasiku,
Department of Physics, Ajayi Crowther University, Oyo-Town, Nigeria,
Email: ayenitaiwobukola@gmail.com

Peer-Review History
Received: 29 April 2025
Reviewed & Revised: 16/May/2025 to 27/February/2026
Accepted: 07 March 2026
Published: 18 March 2026

Peer-Review Model
External peer-review was done through double-blind method.

Discovery
pISSN 2278–5469; eISSN 2278–5450

The influence of corrugation amplitude on entropy production of turbulent flow in outward corrugated converging pipes

Taiwo Bukola Fasiku[1]*, Ayobami Jeremiah Awodunmila[2]

ABSTRACT

This study investigated the entropy production rate of turbulent distilled water flowing through three corrugated converging pipes of various corrugation amplitudes. The impact of the corrugation amplitude $(0.02 \leq e/D \leq 0.03)$ and Reynolds number $(0.5 \times 10^4 \leq Re \leq 4.0 \times 10^4)$ on entropy production rate (EPR) and Bejan number were examined. The finite volume method was utilised to solve the governing equations and the turbulent model (SST $k-\omega$ model), taking into account the boundary conditions stated in the ANSYS Fluent. The findings showed that increasing the corrugation amplitude and Reynolds number reduces the thermal entropy production rate, S_{ther}, compared to a straight pipe. On the contrary, as the aforementioned parameters increase the viscous entropy production, S_{visc}, increases. Therefore, using corrugated converging pipe with enhance corrugation amplitude reduces the entropy production rate compared to a straight pipe.

Keywords: Improvement, Entropy production, Reynolds number, Corrugation, Convergence

1. INTRODUCTION

The convective heat transfer efficiency of various heat systems, such as solar collectors, energy storage systems, nuclear and chemical, fuel cells, and the food industry, can only be efficient if optimisation is carried out (Kaood et al., 2024). This optimisation involves using two common techniques: passive and active techniques. Over some decades, the passive technique has gained significant recognition in the area of optimal thermal performance (Mezaache et al. 2023). The improvement of heat transfer in thermal systems has been confirmed through the use of corrugated pipes, dimpled tubes, and helical coil inserts, as studied by numerous authors (Zheng et al., 2022; Khashaei et al., 2023; Sabir et al., 2022; Flayh et al., 2025). In the utilisation process of these thermal systems, two factors are of concern: enhancing the heat transfer rate and minimising the entropy production rate (EPR). The study of entropy production due to free convection in enclosed surfaces has attracted the attention of many engineers (Esmaeili and Rasidi, 2025). Consequently, much research has focused on evaluating thermal performance alongside entropy production in pipe flows. Nonetheless, it is important to note from the second law of thermodynamics

that not all heat generated can be completely recovered and converted into useful work. Some energy is lost during heat and fluid flow, which relates to entropy. However, recent studies have proposed two approaches for improving heat performance, such as converging and corrugated pipes, instead of the traditional (smooth) pipe. Al-Zuhairy et al., (2024) investigated how corrugation characteristics influence pressure drop and heat transfer in different channels. Four sinusoidal wavy channels were experimentally studied under turbulent flow with specified heat fluxes, geometric parameters, and Reynolds numbers ($1.93 \times 10^3 - 3.29 \times 10^3$). The turbulent flow in rod-baffled corrugated tubes at various corrugation amplitudes was investigated by Fadhil et al., (2023). The impact of Reynolds number, corrugation ratio, pitch of the corrugation, and rod-baffle gap on heat transfer and pressure drop (ΔP) were reported. They observed that corrugation led to the formation of a primary vortex at the centre of the tube, while a secondary vortex formed near the pipe wall. These vortices depleted the thermal boundary layers and improved fluid mixing. The average Nusselt number increased by 25% and 55% at corrugation pitch (10 mm) and corrugation ratios, respectively. However, the flow was accompanied by a higher friction factor than in a smooth pipe.

Ekiciler (2024) numerically investigated the thermal transfer and flow resistance of a hybrid nanofluid flowing in a 2D pipe under a turbulent flow regime. The study reported the impact of various surface corrugation patterns (increasing, decreasing, and non-uniform corrugations), a volume fraction of 1% and the Reynolds number. The findings indicated that, at Reynolds number 28000, for the aforementioned patterns, the Nusselt number values were 134%, 146%, and 137%, respectively. However, the non-uniform surface groove had the maximum friction factor, while the increasing-wall corrugation pipe had the least friction factor and the optimal thermal performance. Ahmad et al., (2023) analysed the hydrothermal performance of a doubled dimpled corrugated tube using both a single and a hybrid nanofluid. The impact of Reynolds number ($4000 \leq Re \leq 20000$) and volume concentration ($1\% \leq \alpha \leq 3\%$) on heat transfer coefficient, temperature distribution, friction factor and Nusselt number was investigated. The results showed that 3% of hybrid nanofluid gave a 20-25% gain in heat transfer coefficient and was the top-performing nanofluid.

Several studies have been carried out on the entropy production rate with corrugated pipes. Kumar et al. (2023) analysed the variable thermophysical properties of fluid flowing in hybrid corrugated channels in a turbulent flow. The effects of associated variables such as viscosity, density and thermal conductivity on heat transfer, fluid flow and entropy production were examined. The outcome revealed that the use of the corrugated channel and the variable properties substantially affect the Nusselt number. The increase in Reynolds number with variable fluid properties leads to a reduction in the total entropy production. Saoudi and Zeraibi (2023) examined the entropy production and the thermal performance of Al_2O_3/water nanofluid flow through corrugated channels. The impact of different corrugation profiles (sinusoidal and square), particle concentration (0-5%), particle diameter ($10nm \leq \alpha \leq 60nm$) and Reynolds number ($200 \leq Re \leq 800$) on the heat transfer, thermal and frictional entropy production and Bejan number were analysed. The results showed that increasing the particle concentration to 5% with Re (800) and particle diameter (10nm) reduces the total entropy generation in square and sinusoidal and channels by 22.12 % and 28.39 %, respectively. However, as the nanoparticle diameter reduces, the total entropy production in both sinusoidal and square channels is reduced by 34.85 % and 20.5 %, respectively. Fadodun et al., (2022) analysed the EPR of ferrosoferric oxide/water (Fe_3O_4/H_2O) of turbulent nanofluid moving in an outwardly corrugated pipe. The effect of the corrugation profiles (circular, triangular, and trapezoidal), Reynolds number ($0.5 \times 10^4 \leq Re \leq 3.0 \times 10^4$) and nanoparticle concentration (0-3.0 %) on both viscous and thermal entropy generation rate. The outcome revealed that the trapezoidal corrugation pattern has the superior heat transfer performance, with the mean temperature gradient as the main contributor to thermal entropy production rate, but for the viscous entropy production rate, the turbulent temperature gradients contribute the most.

In the aspect of converging pipes, Kaood et al., (2024) evaluated the hydrothermal performance and entropy production of converging tubes with various dimple shapes. The effect of dimple shapes (stepped-conical, cylindrical, conical and spherical), Reynolds number ($0.3 \times 10^4 \leq Re \leq 4.0 \times 10^4$) and diameter ratio ($1 \leq DR \leq 2$) on Bejan number, viscous, thermal and total entropy production are evaluated. The findings revealed that the dimple tube (tube modification) significantly contributed to the hydrothermal performance and entropy generation of the convergent tubes, with the mean thermal enhancement factor (TEF) attributed to stepped-conical dimple shapes at $DR = 1.75$, yielding 7.81% gain. Gönül (2025) examined the heat transfer of a novel microchannel with a wavy sinusoidal convergent-divergent wall with numerical technique. The study considered the effects of wavelengths, pin heights, amplitudes, and Reynolds number on the Nusselt number, Fanning friction factor, and Péclet number. The outcome indicated that higher amplitudes and reduced wavelengths, with moderate pin heights, resulted in tangible improvements in heat transfer.

Wang et al. (2023) investigated the heat transfer efficiency of turboshaft engines with converging-diverging film holes. The inclination angle, aperture, and blowing ratio showed a significant effect on the separation within the hole, which in turn influenced heat transfer efficiency. In addition, at a maximum of these parameters, the converging-diverging configuration lowered the wall

temperature by 100K. Zada et al. (2024) studied the heat transfer performance of engine oil flowing within a hybrid nanoparticle-fluid in a convergent and divergent channel. The research varied velocity profiles under different Hartmann numbers. In the convergent pattern, a higher porosity results in a higher temperature field. Entropy production was reported to increase with Eckert and Hartmann numbers in both converging and diverging channels.

Fadodun et al., (2024) studied the EPR and hydrothermal efficiency of a hybrid nanofluid (rGO-CO_3O_4/H_2O) passing through corrugated converging pipes. The authors analysed the influence of nanoparticle concentration ($0 \leq VR \leq 0.2$ %), Reynolds number ($0.5 \times 10^4 \leq Re \leq 5.0 \times 10^4$), corrugation profiles (outwardly and inwardly), and diameter ratio ($1 \leq DR \leq 2$) on the EPR, Poiseuille number, mean Nusselt number and PEC. The results showed that both the presence of the corrugations and the converging geometry contributed to an increased Nusselt number compared to smooth pipes. The EPR due to the temperature gradient in the enhanced pipes was lower than that of the smooth pipe, but the opposite is the case for EPR due to fluid flow. Fadodun and Fadodun (2024) examined the entropy generation and thermal performance of distilled/H_2O flowing through outwardly corrugated converging pipes in turbulent flow. The authors explored the effect of the diameter ratio on the behaviour of the performance parameter in relation to the Reynolds number. The study considered the impact of the Reynolds number ($0.5 \times 10^4 \leq Re \leq 5.0 \times 10^4$) and diameter ratio ($1 \leq DR \leq 2$) on the heat transfer performance and EPR. The outcome revealed that increasing Re and DR improved the mean Nusselt number, EPR and Poiseuille number. However, reductions were reported for Bejan number, thermal effective number and PEC. This study aimed to investigate the impact of Reynolds number and corrugation amplitude on the entropy production rates and Bejan number using a compound technique.

2. MATERIALS AND METHODS

Tube geometry modifications

The study examined the heat transfer performance of distilled water passing through an outwardly corrugated converging pipe in the turbulent regime. Fig. 1(a) illustrates the three-dimensional (3D) pipe used in this work. The examined pipe length was constructed to vary the size of the inlet to outlet diameter while keeping the surface area and the total sum of both the inlet and outlet diameters constant. Thus, the 3D is reduced to 2D in order to reduce cost and computational time; therefore, Fig. 1(b) and (c) show the 2D axisymmetric model geometries. The evaluation is carried out under a fully developed turbulent flow regime. The geometrical dimensions of the corrugated pipes used and the diameter ratio (DR) of the converging pipes are presented in Tables 1 and 2, respectively.

Governing Equations

The steady state governing equations for solving the flow problem are the continuity, momentum and energy equations (Ajeel et al., 2019) and are expressed as:

Continuity Equation:

$$\frac{\partial}{\partial x_i}(\rho u_i) = 0 \tag{1}$$

Momentum Equation

$$\frac{\partial}{\partial x_j}(\rho u_i u_j) = -\frac{\partial P}{\partial x_i} + \frac{\partial}{\partial x_j}\left[\mu\left(\left(\frac{\partial u_i}{\partial x_j} + \frac{\partial u_j}{\partial x_i}\right) - \frac{2}{3}\frac{\partial u_i}{\partial x_j}\delta_{ij}\right)\right] + \frac{\partial}{\partial x_j}\left(-\rho\overline{\acute{u}_i\acute{u}_j}\right) \tag{2}$$

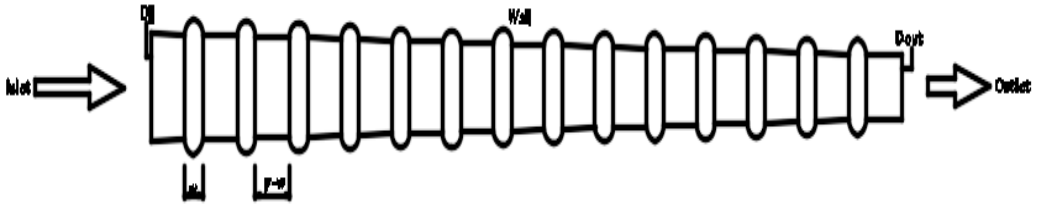

Figure 1(a). The outwardly Corrugated Converging Pipe (3D geometry)

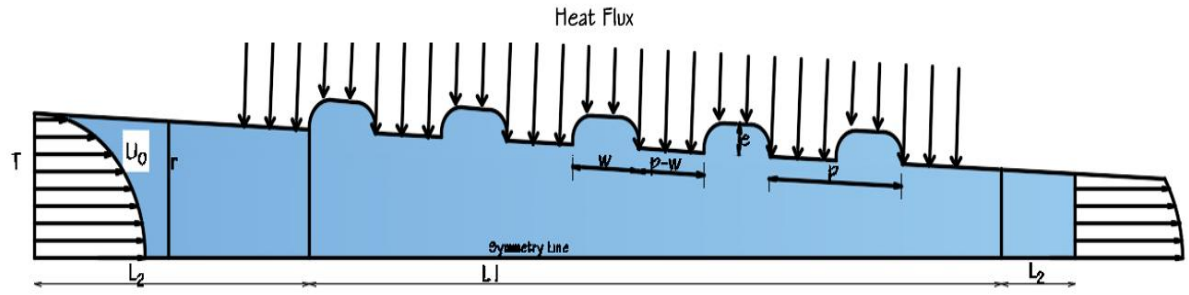

Figure 1(b). 2D Axisymmetric Model

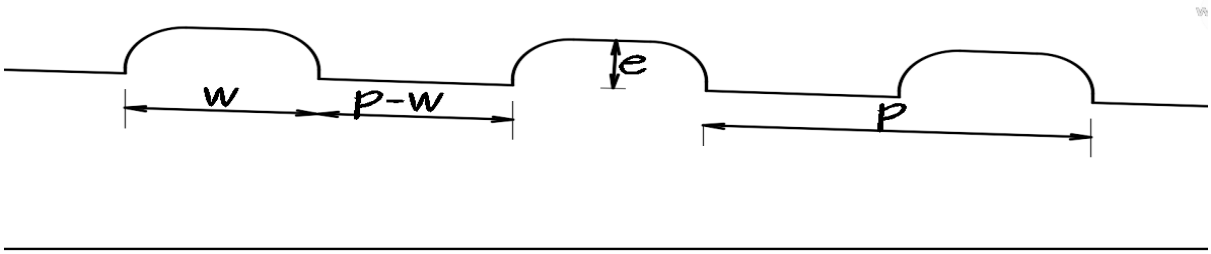

Figure 1(c). Description of the Geometric Parameters

Table 1. The Corrugation Parameters

Parameter	Values (mm)
Corrugation amplitude $\left(\frac{e}{D}\right)$	0.02, 0.025, & 0.03
Corrugation width $\left(\frac{w}{D}\right)$	0.2
Trough between two corrugations $\left(\frac{p-w}{D}\right)$	0.6
Pipe Length (L)	0.4
Pipe Diameter (D)	0.03 m

Table 2. The Diameter ratio (DR) used for the study

$DR = \frac{D_{in}}{D_{out}}$	$D_{in}(m)$	$D_{out}(m)$
1	0.015	0.015
1.2	0.01636	0.01386

Energy equation

$$\frac{\partial}{\partial x_i}[u_i(\rho E + P)] = \frac{\partial}{\partial x_j}\left[\left(\lambda + \frac{C_P \mu_t}{Pr_t}\right)\frac{\partial T}{\partial x_j} + u_i(\tau_{ij})_{eff}\right] = 0 \quad (3)$$

The deviatoric stress tensor (τ_{ij}) is expressed as

$$(\tau_{ij})_{eff} = \mu_{eff}\left[\left(\frac{\partial u_j}{\partial x_i} + \frac{\partial u_i}{\partial x_j}\right) - \frac{2}{3}\frac{\partial u_i}{\partial x_j}\delta_{ij}\right] \quad (4)$$

where, u is the velocity, P denotes the pressure, ρ is the density of the liquid, μ is the dynamic viscosity, μ_t is the turbulent viscosity, C_P defines the specific heat capacity, E represents total energy, k is the thermal conductivity, T is the temperature, Pr_t is the turbulent Prandtl number, λ is the thermal conductivity and $\rho\overline{\acute{u}_i\acute{u}_j}$ denotes the Reynolds tensor stress.

The Shear Stress Transport (SST) $k-\omega$ model was used to close the governing equations for the simulation of the flow in corrugated converging pipes due to its superior capability in accurately modelling in corrugated tubes, as reported in previous studies (Al-Obaidi and Alhamid, 2021; Li et al., 2023; Al-Obaidi, 2025) by providing consistent results with experimental methods. The dissipation rate (ω) and turbulence kinetic energy (k) equations are given by Menter (1994). The thermal and physical parameters of the distilled water used in this study are presented in Table 4.

$$\frac{\partial}{\partial x_i}(\rho k u_i) = \frac{\partial}{\partial x_j}\left[\Gamma_k \frac{\partial k}{\partial x_j}\right] + \widetilde{G_\omega} - Y_k \tag{5}$$

$$\frac{\partial}{\partial x_i}(\rho \omega u_i) = \frac{\partial}{\partial x_j}\left[\Gamma_\omega \frac{\partial \omega}{\partial x_j}\right] + G_\omega - Y_\omega + 2(1-F_1)\rho\sigma_{\omega,2}\frac{1}{\omega}\frac{\partial k}{\partial x_i}\frac{\partial \omega}{\partial x_i} \tag{6}$$

where i and j represent the two coordinates (x and y). The terms G_k and G_ω represent the production of turbulent kinetics due to average velocity gradients and production rates of k and ω. The symbols Y_k and Y_ω represent the turbulent dissipations of k and ω and are written as:

$$Y_\omega = \rho\omega^2\beta_2 \tag{7}$$

$$Y_k = \rho k\omega\beta_1 \tag{8}$$

$$\Gamma_k = \mu + \frac{\mu_t}{\sigma_k} \tag{9}$$

$$\Gamma_\omega = \mu + \frac{\mu_t}{\sigma_\omega} \tag{10a}$$

The terms Γ_k and Γ_ω in Eqs. (3.13) and (3.14) denote the effective diffusivity of k and ω.

$$\sigma_\omega = \frac{1}{\frac{F_1}{\sigma_{\omega,1}} + \frac{(1-F_1)}{\sigma_{\omega,2}}} \tag{10b}$$

The turbulent viscosity (μ_t) is modeled as:

$$\mu_t = \frac{\rho k}{\omega}\frac{1}{\left(\frac{1}{\alpha^*}\frac{SF_2}{\alpha_1\omega}\right)} \tag{11}$$

where the strain rates σ_k and σ_ω are the effective turbulent Prandtl numbers for k and ω, F_1 and F_2 are the blending functions, and α^* is a model constant.

$$\sigma_k = \frac{1}{\frac{F_1}{\sigma_{k,1}} + \frac{(1-F_1)}{\sigma_{k,2}}} \tag{12}$$

$$F_1 = tan({\varphi_1}^4) \tag{13}$$

$$F_2 = tan({\varphi_2}^4) \tag{14}$$

Where,

$$\varphi_1 = min\left[max\left(\frac{\sqrt{k}}{0.09\omega y^+}, \frac{500\mu}{\rho y^{+2}\omega}\right), \frac{4\rho k}{\sigma_{\omega,2}{D^+}_\omega y^{+2}}\right] \tag{15}$$

$${D^+}_\omega = \left[2\times 10^{-20}\frac{\rho}{\sigma_{\omega,2}\omega}\frac{\partial\omega}{\partial x_j}\frac{\partial k}{\partial x_j}\right] \tag{16}$$

$$\varphi_2 = max\left[\left(\frac{2\sqrt{k}}{0.09\omega y}\frac{500\mu}{\rho y^2\omega}\right)\right] \quad (17)$$

The SST $k-\omega$ model constants (Menter, 1994) are presented in Table 3.

Table 3. SST $k-\omega$ turbulent model constants

$\sigma_{k,1} = 1.176$	$\sigma_{k,2} = 1$	$\sigma_{\omega,1} = 2$	$\sigma_{\omega,2} = 1.168$	$\sigma_1 = 0.31$	$\sigma_{i,1} = 0.075$
$\beta_{i,2} = 0.0828$	$\beta_\infty{}^* = 0.09$	$\sigma_\infty = 0.52$	$\sigma_\infty{}^* = 1$	$\beta_i = 0.072$	$\sigma_0 = 1/9$
$R_\beta = 8$	$R_k = 6$	$R_\omega = 2.95$	$\zeta^* = 1.5$	$\sigma_k = 2$	$\sigma_\omega = 2$

Table 4. Thermophysical Properties of the Working Fluid (H_2O)

Type	Thermal Conductivity W/m/K	Density kg/m^3	Specific heat capacity J/kg/K	Dynamic Viscosity kg/m/s
Water	0.602	1000	4200	0.00085

Boundary Conditions

The prescribed velocity ($u_{x,in} = u_{r,in} = 0$) and constant temperature ($T = T_{in} = 300K$) were observed at the inlet section. At the outlet, the pressure gauge was assumed to be zero ($P_{gauge} = 0$, $\frac{\partial u_x}{\partial x} = 0$, $\frac{\partial u_r}{\partial r} = 0$, $\frac{\partial T}{\partial x} = 0$ $\frac{\partial k}{\partial x} = 0$, $\frac{\partial \omega}{\partial x} = 0$). No slip boundary condition ($u_x = 0$, $u_r = 0$) was applied on the wall along the flow direction with constant heat flux ($q'' = 5{,}000\ Wm^{-2}$) was imposed on the upper part of the pipe $\left(\frac{\partial T}{\partial r} = 0\right)$. Both the velocity and temperature gradients were zero at the outlet of the pipe $\left(\frac{\partial u_x}{\partial r} = 0,\ \frac{\partial T}{\partial r} = 0\right)$.

Parameter definitions

The parameters used in this study are the following:

The Reynolds number is given by Li et al. (2022):

$$Re = \frac{\rho D_{in} D_h}{\mu} \quad (18)$$

The inlet velocity (u_{in}) and the mean Nusselt number are expressed as Chaurasiya et al., (2024):

$$u_{in} = \frac{Re\mu}{\rho D_h} \quad (19)$$

$$Nu = \frac{hD_h}{k} \quad (20)$$

$$Nu = \frac{q'' D_h}{(T_{wall} - T_{bulk})k} \quad (21a)$$

The friction factor is expressed as;

$$f = \frac{2D_h \Delta P}{\rho u^2 L}, \quad (21b)$$

Entropy Production Rate (EPR) Analysis

The entropy production rate can be broadly categorised into two types: thermal and viscous entropy production rates. The thermal entropy production rate (TEPR) is caused by temperature gradients, while the viscous entropy production rate (VEPR) is caused by velocity gradients.

The volumetric entropy production rate can be evaluated as Muhammad et al. (2021):

$$S'''_{gen} = S'''_{th} + S'''_{visc} \tag{22}$$

where S'''_{th} and S'''_{visc} are the volumetric thermal and viscous entropy production rate.

The volumetric thermal entropy production rate (S'''_{th}) is expressed as Fadodun and Kaood (2022):

$$S'''_{th} = \left[\frac{\lambda}{T^2}\left(\frac{\partial \bar{T}}{\partial x_i}\right)^2 + \frac{\mu_t}{Pr_t}\frac{Cp}{\bar{T}^2}\left(\frac{\partial \bar{T}}{\partial x_i}\right)^2\right] \tag{23}$$

The average temperature gradient is responsible for the EPR in the first term, whereas the turbulent temperature gradient is attributed to the second term.

The corresponding formula for volumetric viscous entropy production rate (S'''_{th}) is:

$$S'''_{visc} = \frac{\mu}{\bar{T}}\left[2\left(\frac{\partial \bar{V}_i}{\partial x_i}\right)^2 + \left(\frac{\partial \bar{V}_i}{\partial x_j} + \frac{\partial \bar{V}_j}{\partial x_i}\right)^2\right] + \frac{\rho\epsilon}{T} \tag{24}$$

The first expression in Eqn. (24) is due to the mean velocity flow, while the latter is due to the turbulent velocity gradient. To obtain the entropy production rate within the volume, we integrate Eqs. (23) and (24) over volume; then, we have:

$$\dot{S}_{ther} = \iiint_{V_0}^{V_1}\left(\frac{\lambda}{T^2}\left(\frac{\partial \bar{T}}{\partial x_i}\right)^2 + \frac{\mu_t}{Pr_t}\frac{Cp}{\bar{T}^2}\left(\frac{\partial \bar{T}}{\partial x_i}\right)^2\right) dV \tag{25}$$

$$\dot{S}_{visc} = \iiint_{V_0}^{V_1}\left(\frac{\mu}{\bar{T}}\left[2\left(\frac{\partial \bar{V}_i}{\partial x_i}\right)^2 + \left(\frac{\partial \bar{V}_i}{\partial x_j} + \frac{\partial \bar{V}_j}{\partial x_i}\right)^2\right] + \frac{\rho\varepsilon}{T}\right) dV \tag{26}$$

The EPR is the sum of the thermal entropy production rate (TEPR) and viscous entropy production rate (VEPR) and is expressed as:

$$\dot{S}_{gen} = \dot{S}_{ther} + \dot{S}_{visc} \tag{27}$$

The normalized $\dot{S}_{ther}$ and $\dot{S}_{visc}$ can be evaluated by

$$N_{ther} = \frac{(\dot{S}_{ther})_{corr}}{(\dot{S}_{ther})_{smth}} \tag{28}$$

$$N_{visc} = \frac{(\dot{S}_{visc})_{corr}}{(\dot{S}_{visc})_{smth}} \tag{29}$$

$$N_{gen} = \frac{(\dot{S}_{gen})_{corr}}{(\dot{S}_{gen})_{smth}} \tag{30}$$

Where the subscripts cor and $smth$ denote corrugated and smooth tubes, respectively.

Taking a cylindrical pipe with a fixed heat flux, Ratts & Raut (2004) integrated Equations (23) and (24) over the tube length, L, and obtained the entropy production rate $\dot{S}_{gen}$ for a circular straight pipe as:

$$\dot{S}_{gen} = \frac{(\dot{q}'')^2 \pi {D_h}^2 L}{Nuk{T^2}_{av}} + \frac{32\dot{m}^3 fr}{\pi^2 \rho^2 {D_h}^5 T_{av}} \tag{31}$$

The EPR due to thermal flow is the first term on the LHS of Eqn. (20), and the EPR arising from viscous dissipation is the second term.

where, $\dot{q}'', \dot{m}, k, \rho$ and T_{av} are the heat flux, mass flow rate, thermal conductivity, density and average temperature.

Bejan number is a measure of the significance of thermal flow to the overall entropy production rate. It can be evaluated as Bejan, (1982):

$$Be = \frac{\dot{S}_{ther}}{\dot{S}_{gen}} \tag{32}$$

Mesh Generation and Numerical Method

In the flow domain, a non-uniform structural mesh was applied to evaluate the accelerated changes in velocity and temperature gradients ($y^+ \approx 1$) as illustrated in Fig. 2. However, the grid density was concentrated near the wall. In the governing equations, the discretization of the convective term was carried out by the second-order upwind scheme and the diffusion term was performed using the central differencing scheme. The second-order implicit method was used for transient formulation, and the SIMPLE algorithm was employed for pressure-velocity coupling. The discretised equations are solved iteratively, setting the convergence criteria to 10^{-8} for all variables such that:

$$\left|\frac{N^{i+1} - N^{i}}{N^{i+1}}\right| \leq 10^{-8} \tag{33}$$

Grid independence test and validation

A grid independence test is performed by varying the mesh count used to obtain Nusselts number (Nu) of distilled water flowing in the corrugated converging pipe of $DR = 1.6$, $Re = 4.0 \times 10^4$ and $\frac{e}{D} = 0.03$ as depicted in Fig. 3. The relative error for Nu of 341.25 and 336.711, along with the corresponding mesh configurations of 97121 and 211659, are less than 1.5%. This showed that the element configuration of 97121 was the optimum and was adopted for the study.

The numerical model in this study is validated against numerical and experimental studies done by other researchers. For validation purposes, the friction factor (f) and the Nusselt number (Nu) of distilled H_2O flowing in a smooth pipe were evaluated. The results of Nu were compared with the correlations proposed by Gnielinski (1976) in Equation (34).

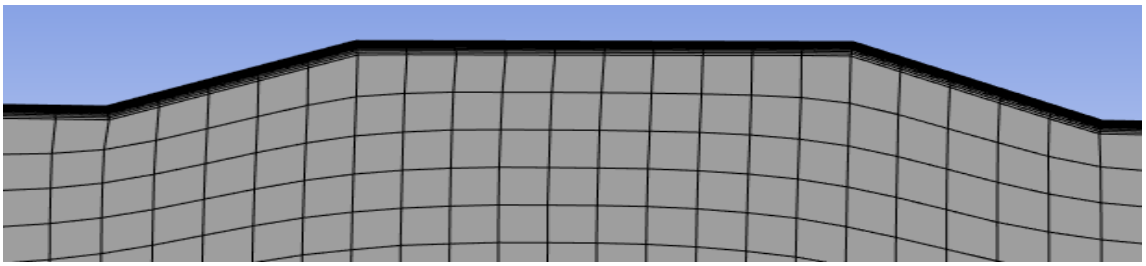

Figure 2. Mesh captured with Boundary Layer

In contrast, the results of f were compared with the correlations obtained by Filonenko (1954) and Blasius (1913) in Equations (35) and (36), respectively. The results of the correlation of Nu is shown in Fig. 4 and f in Fig. 5, a strong correlation was observed between them.

$$Nu = \frac{\left(f/8\right)(Re - 1000)Pr}{1 + 12.7\left(f/8\right)^{0.5}\left(Pr^{2/3} - 1\right)} \tag{34}$$

$$f = (1.82log_{10}Re - 1.64)^{-2} \tag{35}$$

$$f = \frac{0.316}{Re^{0.25}} \qquad for\ Re \leq 2 \times 10^4 \tag{36}$$

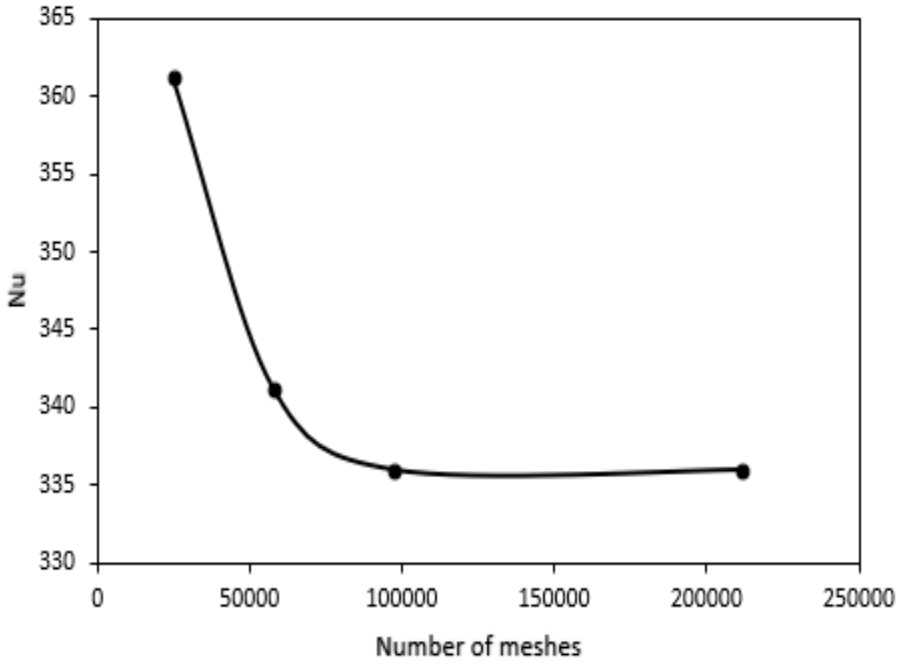

Figure 3. The plot of Nusselt number against the number of meshes (grid independence test)

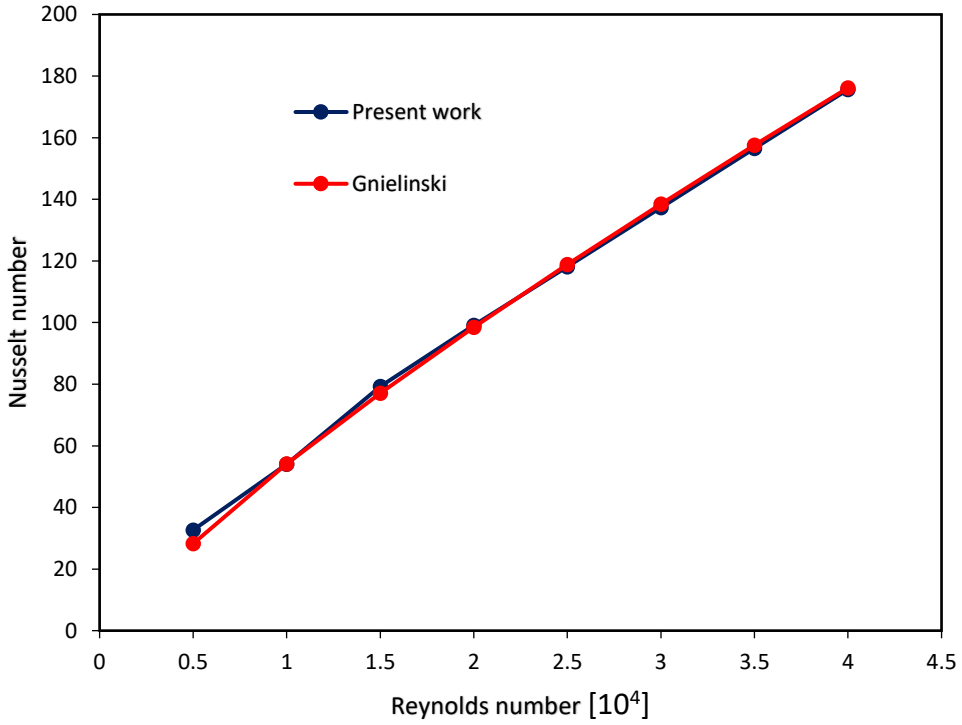

Figure 4. The graph of the Nusselt against the Reynolds number

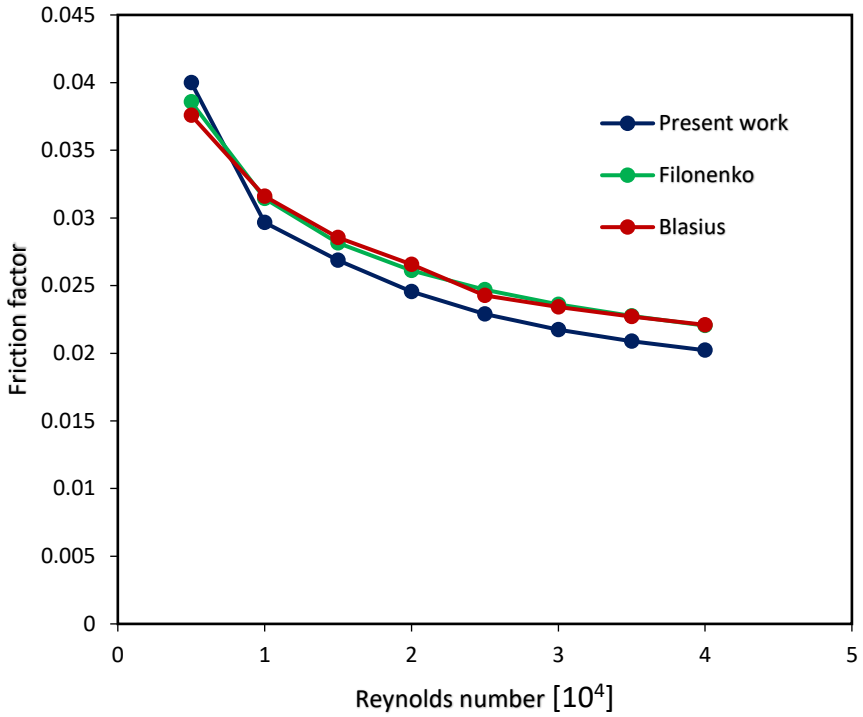

Figure 5. The relation of the friction factor to Reynolds number

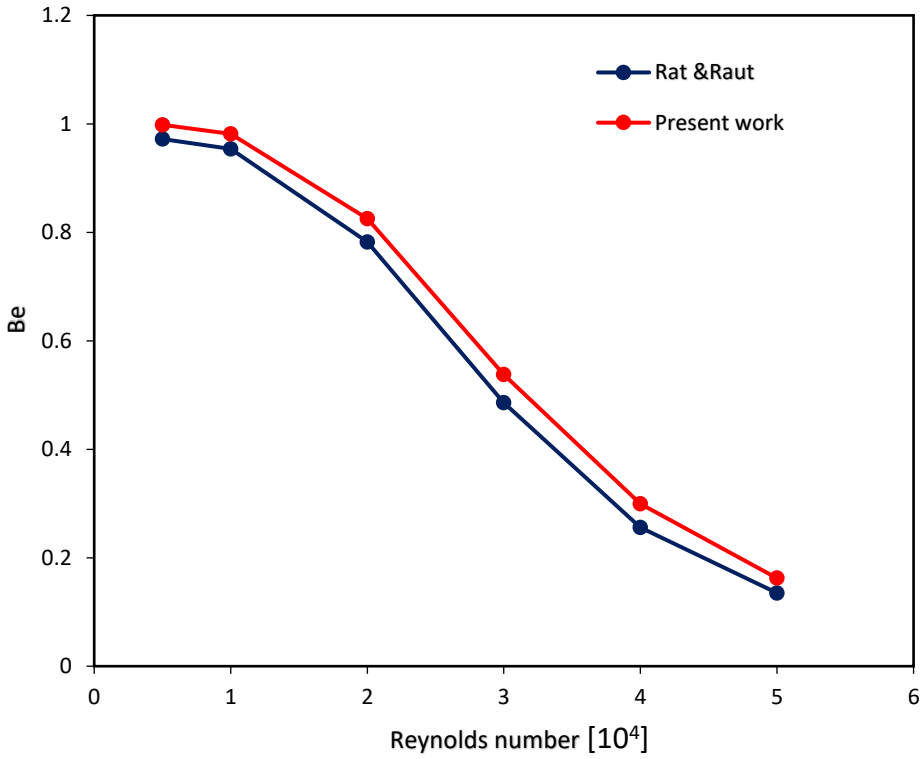

Figure 6. Variation of Bejan number (*Be*) against Reynolds number

Furthermore, the Bejan number of distilled water flowing through a straight pipe was compared with the correlation presented by Ratt and Rauts (2004) in Eqn. (31). Fig. (6) shows the results obtained from the comparison. The two entropy production rate categories such as thermal and viscous entropy production rates are agreed.

3. RESULTS & DISCUSSION

This part examines and analyses the impact of the corrugation amplitude ($0.02 \leq e/D \leq 0.03$) in relation to Reynolds number ($0.5 \times 10^4 \leq Re \leq 4.0 \times 10^4$) on entropy production rate of distilled water flowing in corrugated converging pipes.

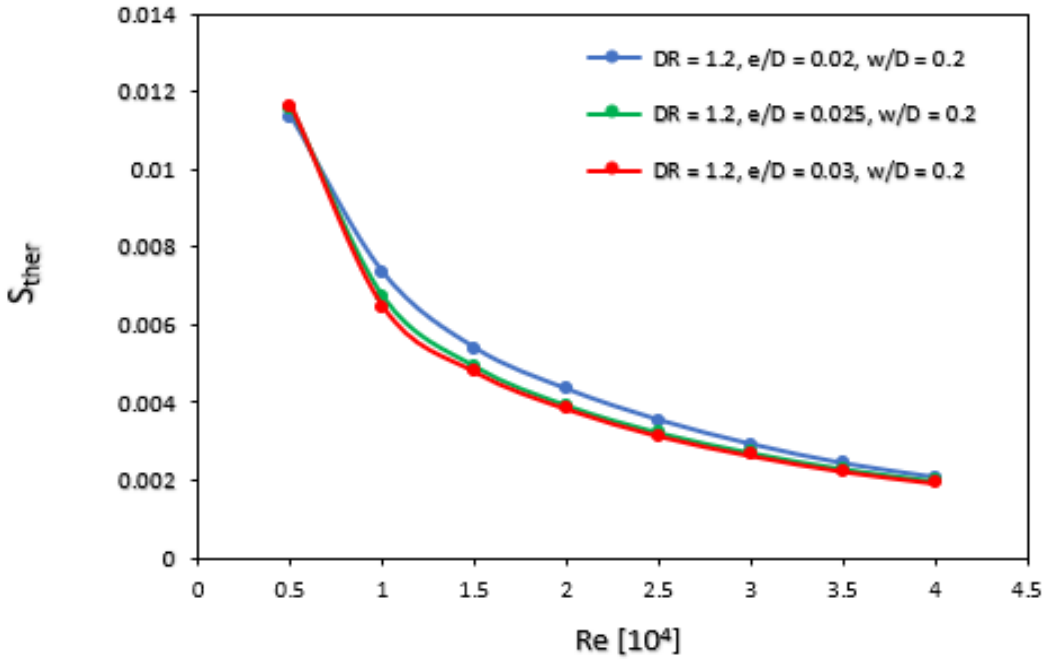

Figure 7. The variation of $\dot{S}_{ther}$ against the Re different corrugation amplitude

Entropy Production Rate

Fig. 7 illustrates the variation of thermal entropy production rate ($\dot{S}_{ther}$) evaluated from Eq. (31) against Reynolds number in different designs of corrugated converging pipes investigated. The impacts of Reynolds number and corrugation amplitude on the thermal entropy production rate are considered. It is observed that increasing Reynolds number diminishes the $\dot{S}_{ther}$ values. For instance, at $Re = 5.0 \times 10^3$, $\frac{e}{D} = 0.02$, $DR = 1.2$ and $\frac{w}{D} = 0.2$, the value of $\dot{S}_{ther}$ is 0.0113 WK^{-1}, whereas the corresponding value at $Re = 4.0 \times 10^4$ is 0.0021 WK^{-1}. This is due to a decrease in the thickness of the TBL as the Reynolds number increases, which improves heat transfer performance. This makes the temperature gradient (∇T) in the flow field as a key factor in $\dot{S}_{ther}$, as presented in Eqn. (25), to be gradual with a non-zero value within the TBL. Thus, it causes a reduction in $\dot{S}_{ther}$. For a clearer explanation, the $\dot{S}_{ther}$ model provided by Ratt and Raut in Eq. (31) showed that $\dot{S}_{ther}$ is inversely proportional to the Nusselt number (Nu), and higher Reynolds number enhances Nu , resulting to reduction in the thermal entropy production rate. Considering the impact of corrugation amplitude $\left(\frac{e}{D}\right)$ on $\dot{S}_{ther}$ from the same figure, it can be recorded that increasing corrugation amplitude lowers the $\dot{S}_{ther}$. The TEPR reduces as the corrugation amplitude rises from 0.02 to 0.03 for $Re > 5000$. For instance, at $Re = 4.0 \times 10^4, DR = 1.2$ and $\frac{w}{D} = 0.2,$, the values of $\dot{S}_{ther}$ in the configurations of $\frac{e}{D} = (0.02, 0.025 \ \& \ 0.03)$ are 0.0021, 0.0020 and 0.0019 WK^{-1}, respectively. As the corrugation amplitude increases, the residence time of the flow increases, resulting in higher flow resistance and enhanced turbulence. The reduction in the cross-sectional area as the pipes converge resulted to rapid axial velocity of the flow, which in turn reduces the TBL and improves the Nu. Consequently, $\dot{S}_{ther}$ is reduced.

Fig. 8 depicts the graph of normalized thermal entropy production rate, N_{ther} evaluated by Eq. (28) (fraction of $\dot{S}_{ther}$ in modified pipes to the respective straight pipe) in relation to the Reynolds number. The result demonstrated a decrease in the N_{ther} as the

Reynolds number appreciates. At $Re = 2.0 \times 10^3$ across the corrugation amplitude 0.02, 0.025 and 0.03, the N_{ther} values obtained are 0.835, 0.755 and 0.739, respectively.

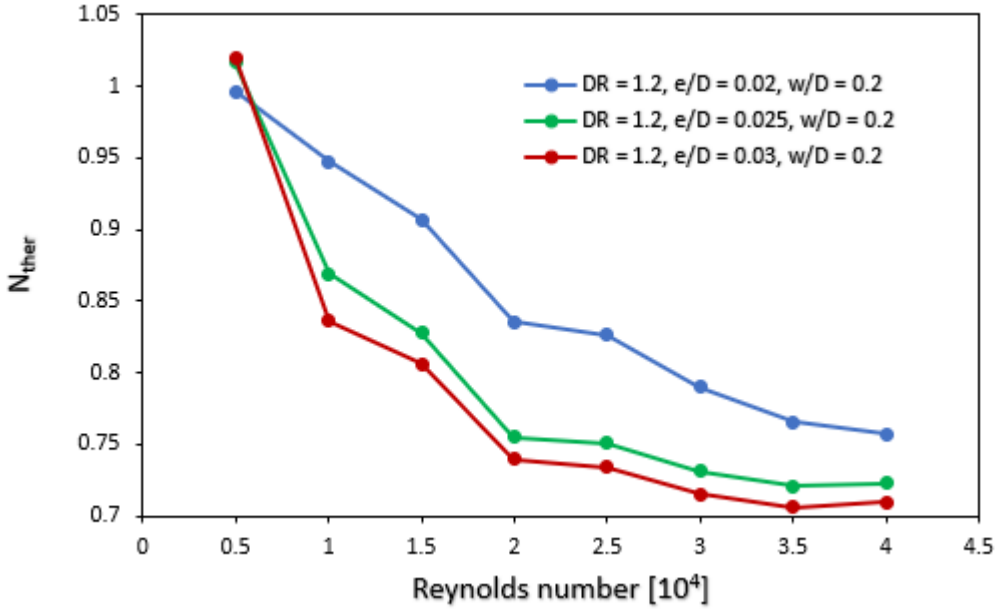

Figure 8. Variation of N_{ther} against the Reynolds number

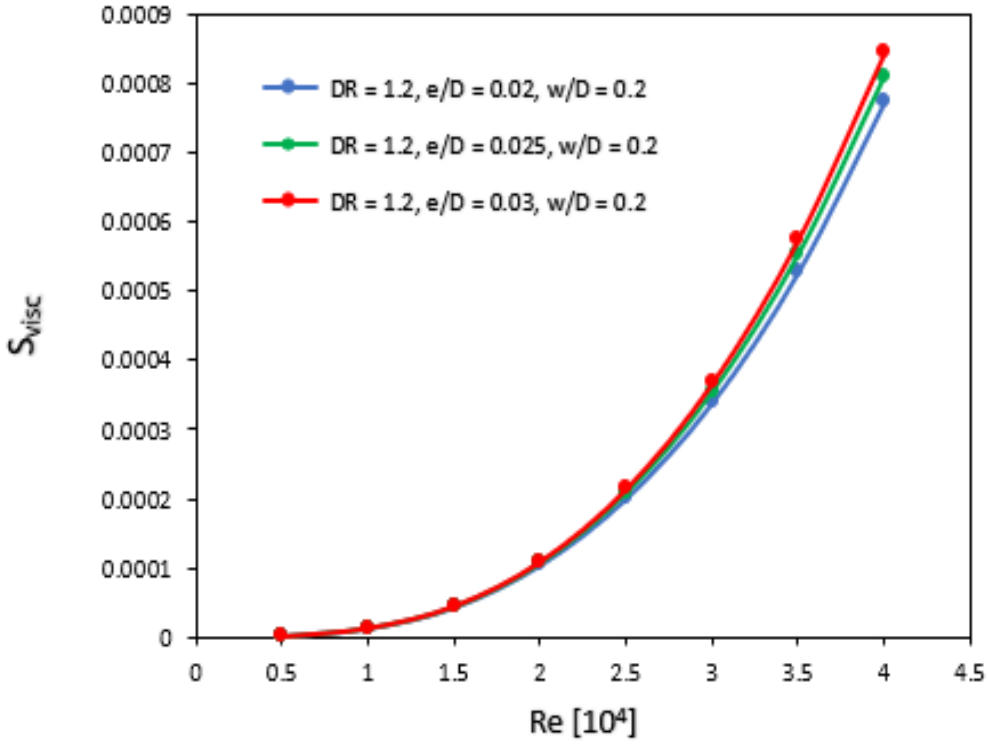

Figure 9. The variation of $\dot{S}_{visc}$ against the Re with varying corrugation amplitude

Fig. 9 depicts the distribution of the viscous entropy production rate $(\dot{S}_{visc})$ estimated from Eq. (31) against the Reynolds number in the modified pipes evaluated. The plot showed that a rise in Reynolds number improves the $\dot{S}_{visc}$. For example, at $Re = 5.0 \times 10^3$, $\frac{e}{D} =$

0.02, $DR = 1.2$ and $\frac{w}{D} = 0.2$, the value of $\dot{S}_{vic}$ is 2.06×10^{-6} WK^{-1}, where the corresponding value at $Re = 4.0 \times 10^4$ is 0.00077 WK^{-1}. This is due to a higher velocity gradient and eddy dissipation rate (ϵ) as Reynolds number increases. This is further explained by Ratt and Raut in Equation (31), which states that an increase in $\dot{S}_{visc}$ is proportional to the cube of the mass flow rate ($\dot{m}^3$), that is Re is proportional to $\dot{m}$. In the figure as well, it is observed that increasing the corrugation amplitude ($\frac{e}{D}$) increases the $\dot{S}_{visc}$. For instance, at $Re = 4.0 \times 10^4, DR = 1.2$ and $\frac{w}{D} = 0.2$, the values of $\dot{S}_{visc}$ in the configurations of $\frac{e}{D} = (0.02, 0.025$ and $0.03)$ are 0.00077, 0.00082, and 0.00085 WK^{-1}, respectively. This is because an increase in corrugation amplitude and convergence of the pipe exerts more resistance against the flow, leading to a higher turbulence flow rate, which in turn rises the velocity gradient and eddy dissipation rate. Alternatively, from Eq. (31), $\dot{S}_{visc}$ is proportional to the friction factor (f). Therefore, an increase in corrugation amplitude enhances f, which increases the $\dot{S}_{visc}$.

Fig. 10 illustrates the variation of the normalised viscous entropy production rate, N_{visc} calculated from Eq. (29) (fraction of $\dot{S}_{visc}$ in configured pipes to the respective straight pipe) against the Reynolds number. The result showed that increasing the Reynolds number enhances the N_{visc}. For instance, at the Reynolds number 2.0×10^3 across the corrugation amplitude considered (0.02, 0.025 and 0.03), the N_{visc} values obtained are 1.35, 1.39 and 1.41, respectively.

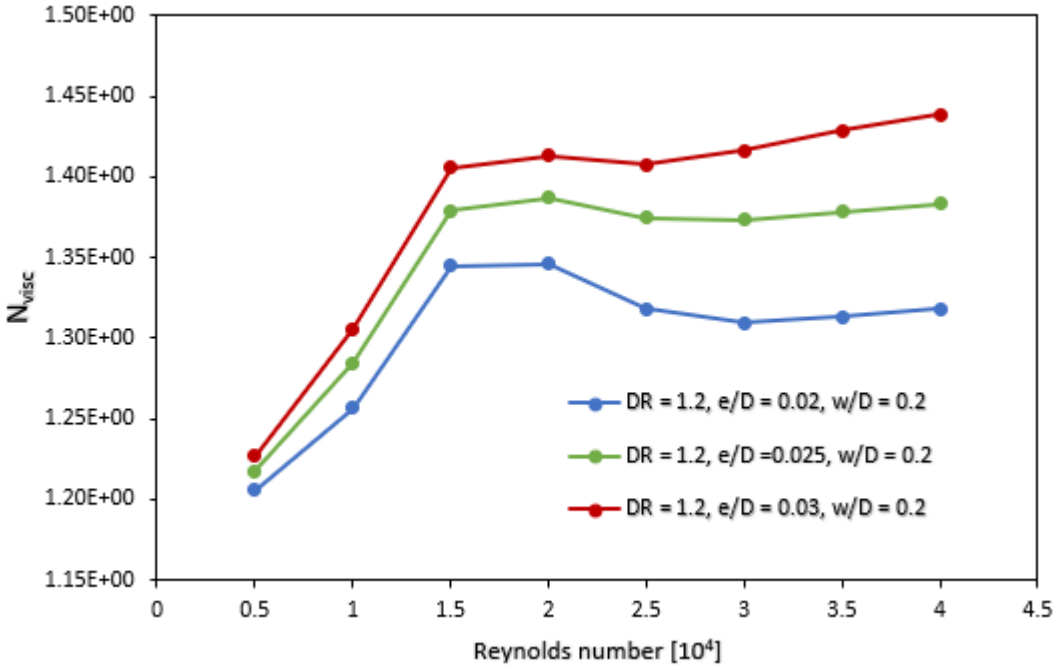

Figure 10. Variation of N_{visc} against the Reynolds number

Fig. 11 shows the plot of total entropy production rate evaluated from Eq. (31) against the Reynolds number in the configured pipes studied. The influence of Reynolds number and corrugation amplitude on entropy generation rate ($\dot{S}_{gen}$) is investigated. This graph shows that increasing the Reynolds number reduces the $\dot{S}_{gen}$ values. For instance, at $Re = 5.0 \times 10^3$, $\frac{e}{D} = 0.02$, $DR = 1.2$ and $\frac{w}{D} = 0.2$, the value of $\dot{S}_{gen}$ is 0.0113 WK^{-1}, where the corresponding value at $Re = 4.0 \times 10^4$ is 0.0029 WK^{-1}. The reduction in total entropy production rate with higher Reynolds number is attributed to the predominance of thermal entropy production rate over viscous entropy production rate, where the decrease in $\dot{S}_{ther}$ exceeds the increase in $\dot{S}_{visc}$. On the same profile, the effect of the corrugation amplitude on $\dot{S}_{gen}$ was considered. It is observed that increasing the corrugation amplitude leads to a reduction in the $\dot{S}_{gen}$ values. This reduction is attributed to enhanced convective mixing, which substantially reduces the $\dot{S}_{ther}$ despite a concurrent increase in $\dot{S}_{visc}$.

Fig. 12 shows the correlation of the normalised total entropy production rate, N_{gen} as a function of Reynolds number. The N_{gen} was evaluated using Eq. (30). The result showed a rise in the N_{gen} as the Reynolds number enhances. At Reynolds number 2.0×10^3 across the corrugation amplitude considered, (0.02, 0.025 and 0.03), the N_{gen} values obtained are 1.35, 1.39 and 1.41, respectively.

Fig. 13 illustrates the variation of the Bejan number (Be) evaluated by Eq. (32) against the Reynolds number of corrugated converging pipes. It is observed that enhancing the Reynolds number lowers the Be values. At $Re = 5.0 \times 10^3$, $\frac{e}{D} = 0.02$, $DR = 1.2$ and $\frac{w}{D} = 0.2$, the value of $\dot{S}_{gen}$ is 0.9998, whereas the corresponding value at $Re = 4.0 \times 10^4$ is 0.7284.

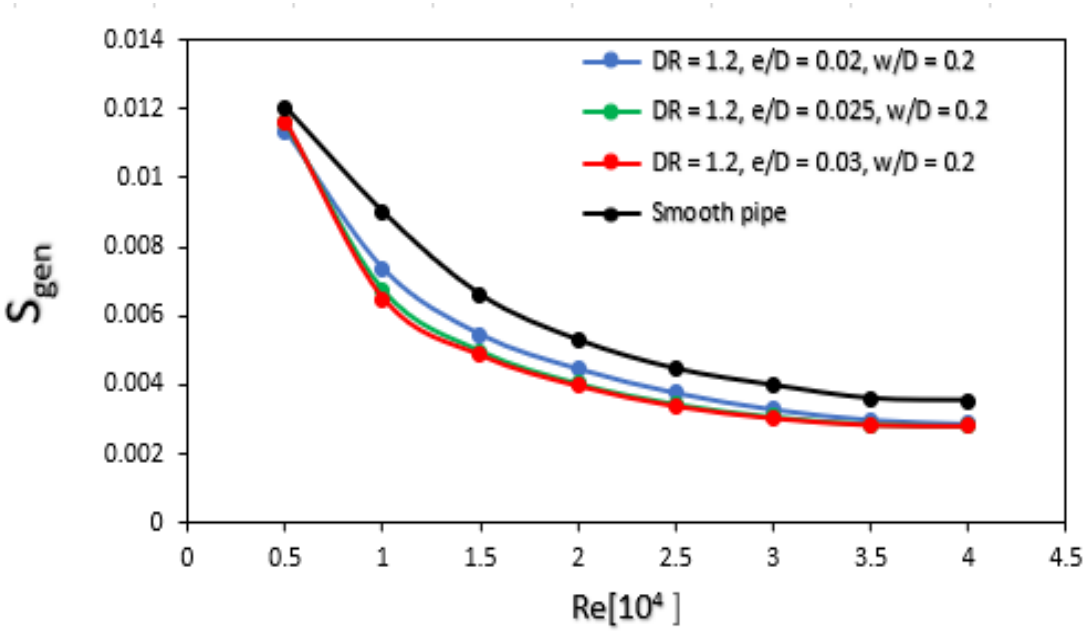

Figure 11. Graph of $\dot{S}_{gen}$ against Re with Varying Amplitude

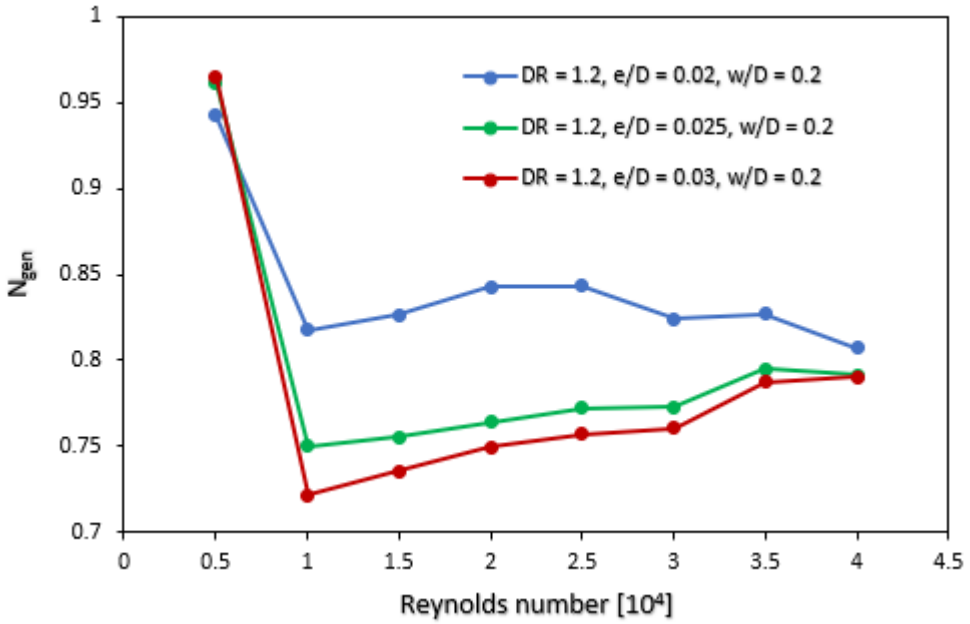

Figure 12. The graph of N_{gen} against Reynolds number

However, there is a decrease in Bejan number in corrugated converging pipes compared to a straight pipe. This decrease is ascribed to enhanced flow velocity accompanied by a higher pressure drop, which leads to increased $\dot{S}_{visc}$ but decreases $\dot{S}_{ther}$. On the same profile, an increasing corrugation amplitude decreases the Bejan number. For instance, at $Re = 4 \times 10^4, DR = 1.2$ and $\frac{w}{D} = 0.2$, the values of Be in the configurations of $\frac{e}{D} = (0.02, 0.025 \text{ \& } 0.3)$ are 0.7284, 0.7094, and 0.6970, respectively. This outcome is expected as a

rise in $\frac{e}{D}$ results in a higher $\dot{S}_{visc}$ but a lower $\dot{S}_{ther}$ and consequently leads to a lower Be. Furthermore, Bejan number values decrease in corrugated converging pipes compared to a straight pipe.

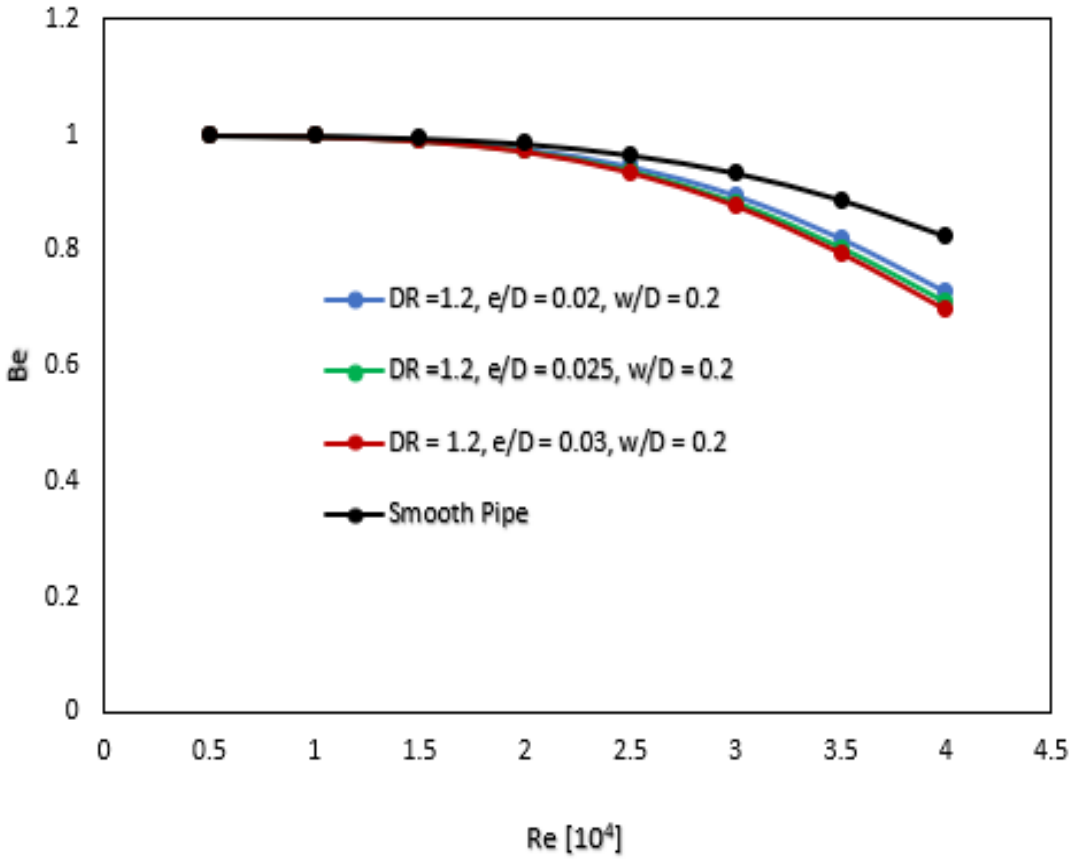

Figure 13. Graph of Be against Re with Varying Amplitude

4. CONCLUSION

In this study, the entropy production rate of corrugated converging pipes with various corrugation amplitude were numerically analysed using the finite volume method. The effects of Reynolds number and corrugation amplitude on thermal and viscous entropy production rate and Bejan number were discussed in detail. The results are summarised below:

- Thermal entropy production rate reduces as the corrugation amplitude of the corrugated converging pipe increases for all values of Reynolds number. The normalized thermal entropy production rate in the various corrugation amplitudes (0.02, 0.025 and 0.03) are 0.835, 0.755 and 0.739, respectively.
- The viscous entropy production rate increases as the corrugation amplitude increases from 0.02 to 0.03 at $Re > 5000$. The N_{visc} values at 2.0×10^3 across the corrugation amplitude (0.02, 0.025 and 0.03) considered are 1.35, 1.39 and 1.41, respectively.
- From the total entropy production rate, the corrugation amplitudes 0.025 and 0.03 coincided from Reynolds numbers 25000 to 40000.
- Increase in corrugation amplitude and Reynolds number lowers the Bejan number. At $Re = 4 \times 10^4, DR = 1.2$ and $\frac{w}{D} = 0.2$ with the corrugation amplitude considered $(0.02, 0.025$ & $0.3)$ the Be values are 0.7284, 0.7094, and 0.6970, respectively.

Nomenclature

e/D	Corrugation amplitude
C_p	Specific heat capacity at constant pressure $[J\ kg^{-1}K^{-1}]$
Nu	Nusselt number
Re	Reynolds number
Pr_t	turbulent Prandtl number

Be	Bejan number
S'''_{gen}	volumetric entropy production $[W\ K^{-1}m^{-3}]$
$\dot{S_{gen}}$	total entropy production rate $[W\ K^{-1}]$
ω	specific dissipation rate $[\ kgm^{-1}s^{-1}]$
k	turbulent kinetic energy $[m^2\ s^{-2}]$
q''	heat flux $[W\ m^{-2}]$
dP	pressure drop $[Nm^{-2}]$
y^+	non-dimensional wall parameter of distance
Y_k	turbulent dissipation of k $[J\ kg^{-1}]$
G_k	rate of production of k $[J\ kg^{-1}]$
λ	thermal conductivity $[W\ m^{-2}\ K^{-1}]$
Γ_k	effective diffusion of k $[kg\ m^{-1}\ s^{-1}]$
Γ_ω	effective diffusion of ω $[kg\ m^{-1}\ s^{-1}]$
G_k	generation of turbulent kinetic of k $[kg\ m^{-1}\ s^{-1}]$
G_ω	generation of turbulent kinetic of w $[kg\ m^{-1}\ s^{-1}]$
ρ	density $[kg\ m^{-3}]$
D	tube diameter $[m]$
μ_t	turbulent viscosity $[kg\ m^{-1}\ s^{-1}]$
ϵ	Eddy dissipation rate $[m^2\ s^{-3}kg]$

Abbreviations

CHTP	convective heat transfer performance
DR	diameter ratio
PEC	performance evaluation criterion
TBL	thermal boundary layer
VEPR	viscous entropy production rate $[WK^{-1}]$
EPR	entropy production rate $[WK^{-1}]$
TEPR	thermal entropy production rate $[W\ K^{-1}]$

Acknowledgement

We would like to express my sincere gratitude to all those who supported me throughout the course of this research.

Author Contributions

Taiwo Bukola Fasiku: Conceptualisation, design, investigation, data acquisition, data analysis and interpretation, writing original draft, review and editing/critical revision.

Ayobami Jeremiah Awodunmila: writing original draft.

Informed consent

Not applicable.

Conflicts of interests

The authors declare that they have no conflicts of interest, competing financial interests or personal relationships that could have influenced the work reported in this paper.

Ethical approval & declaration

Not applicable. This article does not contain any studies with human participants or animals performed by any of the authors.

Funding

This research did not receive any external funding like specific grant from funding agencies in the public, commercial, or nonprofit sectors.

Data and materials availability

Data that support the findings of this study are embedded within the manuscript.

REFERENCES

1. Ahmad F, Mahmud S, Ehsan MM, Salehin M. Thermo-hydrodynamic performance evaluation of double-dimpled corrugated tube using single and hybrid nanofluids. International Journal of Thermofluids, 2023; 17:100283.
2. Ajeel KR, Salim WS, Sopian K, Yusoff MZ, Hasnan K, Ibrahim A, Al-Waeli HA. Turbulent convective heat transfer of silica oxide nanofluid through corrugated channels: An experimental and numerical study. International Journal of Heat and Mass Transfer, 2019; 145(1):1-15.
3. Al-Obaidi AR, Alhamid J. Numerical investigation of fluid flow, characteristics of thermal performance and enhancement of heat transfer of corrugated pipes with various configurations. In Journal of Physics: Conference Series IOP Publishing, 2021; 1733(1): 012004.
4. Al-Obaidi AR. Thermal hydraulic flow investigation and thermal performance enhancement of 3D corrugated tubes based on various geometries and DoE analyses. International Journal on Interactive Design and Manufacturing (IJIDeM), 2025; 19(9): 6127-6149.
5. Al-Zuhairy RC, Kareem ZS, Khudhur DS, Balla HH. Corrugation characteristics effect of channel on heat transfer and pressure Drop: Experimental study. International Journal of Heat and Fluid Flow, 2024; 107:109333.
6. Bejan A. Entropy generation through heat and fluid flow. John Wiley & Sons, New York, 1982; 3(1):1-10.
7. Blasius H. Das Aehnlichkeitsgesetz bei Reibungsvorgängen in Flüssigkeiten,Berlin Heidelberg, Berlin, Heidelberg, Heidelberg, Springer, 1913; 3(1): 1-41.
8. Chaurasiya PK, Heeraman J, Singh AP, Madhuri KS, Sharma VK. Numerical exploration of heat transfer and friction factor in corrugated dual-pipe heat exchangers using SiO2 and CuO nanofluids. Thermal Science and Engineering Progress, 2024; 56: 103076.
9. Ekiciler R. Analysis and evaluation of the effects of uniform and non-uniform wall corrugation in a pipe filled with ternary hybrid nanofluid. Arabian Journal for Science and Engineering, 2024; 49(2): 2681-2694.
10. Esmaeili Z, Rashidi S. Entropy production analysis for nanofluid flow through a channel with perforated transverse twisted-baffles. Energy Sources, Part A: Recovery, Utilization, and Environmental Effects, 2025; 47(2): 2041131.
11. Fadhil NA, Al-Dabagh AM, Hatem FF. Numerical Investigation of Heat Transfer and Pressure Drop Characteristics in a Double Pipe Heat Exchanger with Corrugated Tubes and Rod Baffles at Various Reynolds Numbers. International Journal of Heat & Technology, 2023; 41(3).
12. Fadodun OG, Kaood A, Hassan MA. Investigation of the entropy production rate of ferrosoferric oxide/water nanofluid in outward corrugated pipes using a two-phase mixture model. International Journal of Thermal Sciences, 2022; 178: 107598.
13. Fadodun OO, Fadodun OG, Kaood A. Hydrothermal performance and entropy production rate of rGO-CO3O4/H2O hybrid nanofluid in corrugated-converging pipes. International Journal of Thermal Sciences, 2024; 199: 108911.
14. Fadodun OO, Fadodun OG. Hydrothermal performance and irreversibility production of distilled H2O flowing in outwardly-corrugated converging pipes. Numerical Heat Transfer, Part A: Applications, 2024; 1-20.
15. Filonenko GK. Hydraulic resistance of pipes with smooth walls. Journal of Engineering Physics, 1954; 26(8):1009-1013.
16. Flayh SJ, Ismail EM, Mohammed KS, Abdulhussein HA, Karouei SH, Jasim DJ. A numerical study on enhancing heat transfer within helical coils using twisted tape inserts. Case Studies in Thermal Engineering, 2025; 107063.
17. Gnielinski V. New equations for heat and mass transfer in turbulent pipe and channel flow. International chemical engineering, 1976;16(2):359-367.
18. Gönül A. Enhancement of heat transfer characteristics in wavy microchannel heat sinks with streamlined micropins within convergent-divergent flow passages. Applied Thermal Engineering, 2025; 258:124574.
19. Kaood A, ElDegwy A, Aboulmagd A. Hydrothermal and entropy generation performance of convergent tubes with various dimple shapes. International Journal of Thermal Sciences, 2024;197: 108842.

20. Khashaei A, Ameri M, Azizifar S, Cheraghi MH. Experimental investigation on the heat transfer augmentation and friction factor inside tube enhanced with deep dimples. International Communications in Heat and Mass Transfer, 2023; 149 107149.
21. Kumar K, Kumar R, Bharj RS. Entropy generation studies of turbulent fluid flow through novel hybrid corrugated channels with variable thermophysical properties. International Journal of Modern Physics B, 2023; 37(26): 2350303.
22. Li X, Liu S, Mo X, Sun Z, Tian G, Xin Y, Zhu D. Investigation on Convection Heat Transfer Augment in Spirally Corrugated Pipe. Energies, 2023; 16(3): 1063-1072.
23. Li Y, Yu Q, Yu S, Gong B, Zhang J. Numerical investigation of pulsating flow structures and heat transfer enhancement performance in spherical corrugated helical tube. Applied Thermal Engineering, 2022; 213:118647.
24. Menter FR. Two-equation eddy-viscosity turbulence models for engineering applications, AIAA J. 1994;32: 1598–1605.
25. Mezaache A, Louhichi K, Bessaïh R. Numerical investigation of mixed convection and entropy production of nanofluid flow in a corrugated channel using a two-phase mixture model. Heat Transfer, 2023; 52(1): 734-758.
26. Muhammad NM, Sidik NA, Saat A, Asako Y, Japar AA, Musa GH, Yuof NA. Effect of corrugated minichannel variable width on entropy generation for convective heat transfer of alpha-Alumina-water-nanofluid. Journal of Physics: Conference Series, 2021; 2053(1): 1-9.
27. Ratts EB, Raut AG. Entropy generation minimization of fully developed internal flow with constant heat flux. Journal of Heat Transfer, 2004; 126(1):656-659.
28. Sabir R, Khan MM, Imran M, Sheikh NA, Irfan M. Role of transverse dimples in thermal-hydraulic performance of dimpled enhanced tubes. International Communications in Heat and Mass Transfer, 2022; 139, 106435.
29. Wang B, Wang F, Zhang X, Wang J, Xue T. Numerical analysis of cooling efficiency for turboshaft engines with converging-diverging film cooling holes. International Journal of Thermal Sciences, 2023; 185: 108044.
30. Zada L, Ullah I, Alqahtani AM, Nawaz R, Khan H, Alam K. Enhancing energy efficiency and heat transfer performance of engine oil flow through hybrid nanoparticles in convergent/divergent channel. Results in Engineering, 2024;.22:102027.
31. Zheng D, Du J, Wang W, Klemeš JJ, Wang J, Sundén B. Analysis of thermal efficiency of a corrugated double-tube heat exchanger with nanofluids. Energy, 2022; 256:124522.